Tests of the Extended Lee Model Using Three Different Turbine Meters

Jodie G. Pope, John D. Wright, and Sherry D. Sheckels
National Institute of Standards and Technology, Gaithersburg, MD, USA
Tel: 301−975−4586, Fax: 301−258−9201, E−mail: jodie.pope@nist.gov, john.wright@nist.gov, and sherry.sheckels@nist.gov

Abstract

We report additional tests of our "extended Lee model" for calibrating turbine meters. The model accounts for 1) Reynolds number (*Re*) dependent drag and lift, 2) bearing static drag and 3) bearing viscous drag. Initially, we tested this model using a dual−rotor, 2.5−cm−diameter turbine meter and flow measurements spanning a 200:1 range ($50 < Re < 109{,}000$) with liquid mixtures spanning a 42:1 kinematic viscosity range (1.2×10^{-6} m^2 / s $< \nu < 50 \times 10^{-6}$ m^2 / s). The model correlated the volumetric flow data within 3.6 % over the entire *Re* range. The same data had a maximum deviation of 17 % from the commonly used Strouhal versus Roshko (or *Re*) correlation. In this work, we tested the model using three different single−rotor turbine meters with diameters of 2.5 cm, 1.6 cm, and 1.9 cm and flow measurements spanning a 75:1 range ($140 < Re < 102{,}000$) with liquid mixtures spanning a 12:1 kinematic viscosity range (1.2×10^{-6} m^2 / s $< \nu < 14 \times 10^{-6}$ m^2 / s). The model correlates the flow data within 2.3 % for all three meters over the entire *Re* range. The same data had a maximum deviation of 4.8 % from the commonly used Strouhal versus Roshko (or *Re*) correlation. Therefore, the model works well for single−rotor and dual−rotor meters. The model shows that static bearing drag is responsible for fanning (or non−convergence) of multiple−ν calibration curves. However, as with the dual−rotor meter, the model begins to fail at low *Re* numbers where the bearing drags dominate the rotor's behavior, causing corrections as large as 26 % of the calibration factor.

Nomenclature

A	cross sectional area of flow [m^2]
$C'_{\mathrm{D}}(Re)$	fluid drag coefficient that is a function of Reynolds number with turbine geometric constants included [m^{-3}]
C'_{D0}	constant of $C'_{\mathrm{D}}(Re)$ in the laminar rotor boundary layer range [m^{-3}]
$C'_{\mathrm{D}i}$	constants of $C'_{\mathrm{D}}(Re)$ in the transition − turbulent rotor boundary layer range [m^{-3}] with i = 1, 2, 3, or 4
C_{B0}	constant representing the static drag of the ball bearings [kg m^2 / s^2]
C_{B1}	constant representing the viscous drag on the ball bearings [m^3]
C'_{B0}	constant in term representing the static drag of the ball bearings divided by $\overline{r}^2$ [kg / s^2]
C'_{B1}	constant in term representing the viscous drag on the ball bearings divided by $\overline{r}^2$ [m]
d	diameter of the meter casing [m]
f	rotor blade frequency [s^{-1}]
I	moment of inertia of ball bearings [kg m^2]
K	meter factor based on angular frequency, ω / Q [rad / m^3]
K_f	meter factor based on frequency, f / Q [m^{-3}]
K_i	ideal meter factor, ω_{i} / Q [rad / m^3]
Q	volumetric flow [m^3 / s]
$\overline{r}$	root mean square of meter hub and rotor tip radii [m]
Re	Reynolds number = du / ν
Re_{lam}	laminar region Reynolds number
Re_{turb}	turbulent region Reynolds number
$Re_{K\mathrm{peak}}$	*Re* corresponding to the maximum *K* factor of the multiple−ν calibration curves
Ro	Roshko number = $f d^2 / \nu$
St	Strouhal number = $K_f \pi d^3 / 4$
T_{B}	ball bearing retarding torque [kg m^2 / s^2]

T_D torque due to *Re*−dependent forces [kg m^2 / s^2]

T_r retarding torque [kg m^2 / s^2]

$T_{rotation}$ torque due to angular acceleration [kg m^2 / s^2]

u velocity of fluid entering the rotor [m / s^2]

$\overline{\beta}$ average angle between rotor axis and rotor blade corresponding to the root−mean−square radius $\overline{r}$ [rad]

η absolute viscosity [N s / m^2]

v kinematic viscosity = η / ρ [m^2 / s]

ρ density [kg / m^3]

ω angular frequency [rad / s]

ω_i ideal angular frequency [rad / s]

1. Introduction

Turbine flow meters are widely used to measure the flow of valuable fluids such as natural gas and petroleum products. In many cases the meters are calibrated with one fluid and used with another fluid. The property that effects turbine meter calibration is kinematic viscosity defined as the ratio (absolute viscosity) / (density) = $\eta / \rho = v$. Even when a turbine meter is calibrated and used with a single fluid, v might change between the time of calibration and the time of use because v has a strong temperature−dependence. Because there is poor understanding of how v affects turbine meter calibrations, expensive, extra calibrations occur. For instance, in petroleum custody transfer (billing) applications, a turbine meter is field re−calibrated each time the product in the pipeline changes [1]. In other applications, a single turbine meter is used to measure flows of fluids with very different kinematic viscosities such as jet fuel (1.2×10^{-6} m^2 / s) and hydraulic oils (16×10^{-6} m^2 / s to 100×10^{-6} m^2 / s). To ensure accurate flow measurements over such a wide range of kinematic viscosities it is necessary to understand how v effects meter performance and when the effects of v should be considered for low−uncertainty measurements.

Previously, we presented a physical model called "the extended Lee model" (ELM) that explains the influence of v on turbine meter performance [2]. The model is consistent with the common observation that calibrations made using fluids with different values of v coincide at large Reynolds numbers (*Re*) and spread out (fan) at lower values of *Re*; see Figure 1. The model explains the fanning as a consequence of bearing static drag. In our prior work, we tested the ELM using a dual−rotor, 2.5−cm−diameter turbine meter and flow measurements spanning a 200:1 range ($50 < Re < 109{,}000$) with liquid mixtures spanning a 42:1 v range (1.2×10^{-6} m^2 / s < v < 50×10^{-6} m^2 / s). The model correlated the volumetric flow data within 3.6 % over the entire *Re* range. We successfully applied the ELM to measurements taken from each of the rotors separately and the measurements from the sum of the rotors simultaneously. The goal of this paper is to further test the ELM by fitting it to multiple−v calibration curves from meters that differ in size and design from the meter used in our prior paper [2]. We used three single−rotor turbine meters having 8 blades, 4 blades and 6 blades and with nominal diameters of 2.5 cm, 1.9 cm, and 1.6 cm respectively.

Physical models for the turbine meter based on the momentum and airfoil approaches were publish by Lee and his colleagues [3, 4] and by Rubin *et al*. [5] in the 1960s. Their work and others' are included in Baker's turbine meter review article [6] and are described in Ref. [2], where we derived the ELM. These prior works simplified the effects of bearing drag terms because they considered such torques as constant over the *Re* range of interest [3, 4]. Because they simplified the bearing drag terms, they did not explain why multiple−v calibration curves fan at small *Re* values. They focused on the upper end of the meter range, where the meter factor ($K_f = f / Q$) is an approximately linear function of *Re* or the Roshko number (*Ro*). In this region, the calibration data for various kinematic viscosities collapses onto a single calibration curve. To optimize meter design for rangeability and linearity, prior researchers have focused on the relationship between meter geometry and performance. Instead of improving turbine meter design, this work aims to use a physical model to explain the shape of the turbine meter calibration curve and the fanning observed as a function of v at low *Re* values.

Figure 1 shows the multiple−v calibration curves for each of the meters. The solid lines in Figure 1 are the meter factors K calculated from the ELM when coefficients related to *Re*−dependent drag and lift on the rotor and bearing drag are fitted to the measurements. The wide range of flows and kinematic viscosities exposes several phenomena seen in all of the meters and

(a) 2.5−cm Turbine Meter

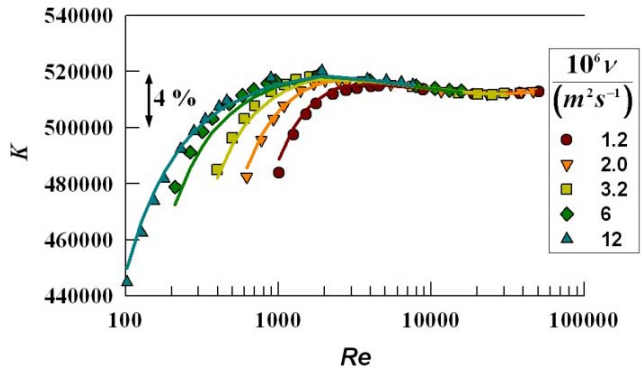

(b) 1.9−cm Turbine Meter

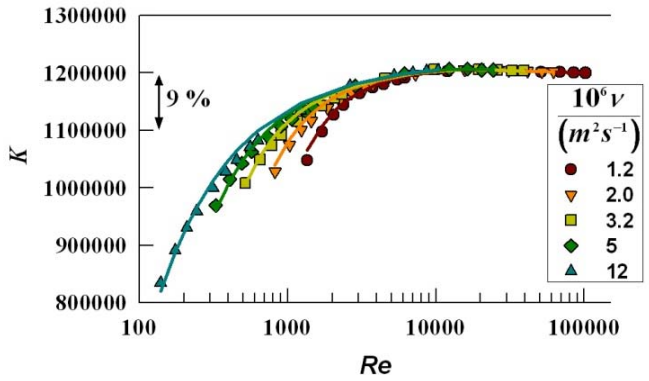

(c) 1.6−cm Turbine Meter

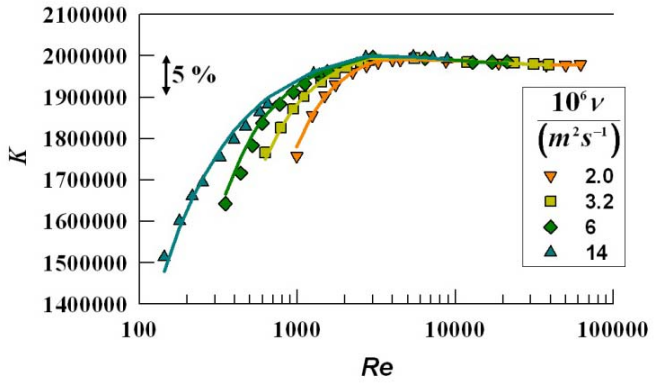

Figure 1: Calibration curve of (a) the 2.5−cm, (b) the 1.9−cm and (c) the 1.6−cm turbine meter with various ν solutions of PG+W. The symbols are measured data and the solid lines are the ELM fit to the data.

that are well explained by the ELM: 1) there is a peak in the meter factor at a *Re* value (*Re* length scale is the inner diameter of the meter casing) that we call $Re_{K\text{peak}}$ that occurs when flow across the rotor changes from laminar to turbulent and is not necessarily coincident with the beginning of the fanning phenomenon, 2) meter factor versus *Re* plots work well in what we call the "ν−independent range" of the turbine meter, where the separation of different ν curves is less than the long term reproducibility of a calibration performed in the same fluid, and 3) at *Re* < a meter specific value, a fanning of the curves occurs. We have named the range of the calibration curve where fanning occurs the "bearing−dependent range" because the bearings are responsible for the fanning phenomenon [2].

2. Materials and Methods

United States Pharmacopeia grade (*i.e.*, safe for human consumption) propylene glycol was mixed with reverse osmosis water to generate mixtures (PG+W) ranging in kinematic viscosity from 1.2×10^{-6} m^2 / s to 14×10^{-6} m^2 / s at 21 °C. The National Institute of Standards and Technology (NIST) 20−L hydrocarbon liquid flow standard was used to generate calibration curves at temperatures between 20 °C and 22 °C [7] for three single−rotor turbine meters having 8 blades, 4 blades and 6 blades and with nominal diameters of 2.5 cm, 1.9 cm, and 1.6 cm respectively. The NIST standard is a piston prover (Figure 2). The motor−driven piston works like a syringe pump. It sweeps a known volume during a known period of time through the cylinder generating a known flow through the meter. The frequency measured from the meter during the known volumetric flow gives the meter specific K_f factor. The prover has a 95 % confidence level uncertainty of 0.074 % (All uncertainties herein are approximately 95 % unless otherwise stated). To avoid cavitation, the system was pressurized to approximately 260 kPa. Data were collected over the range of operation of the NIST 20−L prover (1.5 L / min to 114 L / min). For each PG+W mixture, 5 data points were taken at each flow. For a given flow, meter repeatability ranged from 0.02 % to 0.28 % with the 1.9−cm meter having the worst repeatability.

We determined the ρ and ν of each mixture as a function of temperature. The resulting ρ and ν data agree with other reports of PG+W properties within 1 % [8, 9]. For calibrations, the required accuracy of ν depends upon the *Re* range of the calibration. By definition, low uncertainty is not required in the ν−independent range of the turbine meter [2]. However, accurate ν values are

necessary to obtain low−uncertainty calibrations in the bearing−dependent range. To determine the accuracy required for v in the bearing−dependent range for each meter we computed the partial derivative of the ELM with respect to v, normalized by multiplying by v / K, $(v / K) / (\partial K / \partial v)$. We found that a 1 % error in v will introduce a 0.1 %, 0.3 % and 0.3 % error in the measured flow for the 2.5−cm, 1.9−cm and 1.6−cm turbine meter, respectively, at the lowest *Re* measured.

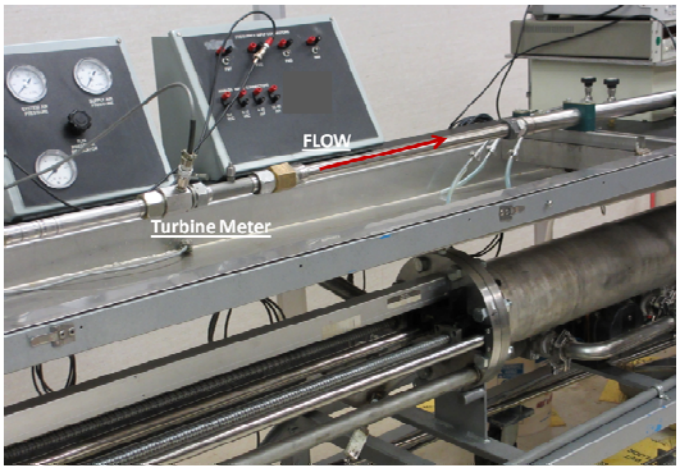

Figure 2: NIST's 20−L piston prover with the 2.5−cm, single−rotor turbine meter installed.

3. Extended Lee Model for the Turbine Flow Meter

The relationship between the fluid flow through a turbine meter and its rate of rotation is dependent on many parameters that are impractical to measure with low uncertainty, *e.g.*, blade angles, tip clearance and bearing friction. Hence our goal is not to derive a physical model that attempts to relate precisely measured meter geometry to the meter calibration. Instead we seek the functional form of the physical model that we can fit to flow calibration data. The model coefficients determined from our test flows and kinematic viscosities during calibration can then be used to interpolate data for other conditions.

In the literature, there are two approaches that account for the calibration curves for turbine flow meters. The first approach describes fluid driving torques in terms of aerodynamic lift and drag via airfoil theory. The second describes it in terms of momentum exchange [10]. We have chosen the momentum approach because it leads to the functional form of the calibration curve without knowledge of the meter's internal geometry. The ELM has been derived in detail previously [2]. The derivation is summarized here starting with the fundamental expression of the turbine meter Lee model based on the momentum approach:

$$K = \frac{\omega}{Q} = \frac{\tan\overline{\beta}}{\overline{r}A} - \frac{T_r}{\overline{r}^2 \rho Q^2}, \qquad (1)$$

where, $\dfrac{\tan\overline{\beta}}{\overline{r}A} = K_i$.

The ideal K factor (first term on the right hand side of Equation 1) is reduced by the retarding torques (second term) to obtain the real K factor.

We previously extended the Lee model by including expressions for the retarding torques related to fluid drag and bearing friction drag. This led to the finding that bearing drag is responsible for the fanning in the multiple−v calibration curves.

3.1. Fluid Drag and Other Reynolds Number Dependent Forces

There are several *Re*−dependent phenomena that influence the shape of turbine meter calibration curves. These include 1) the fluid drag on the entire rotor including that on the blade surfaces, blade tips, and the rotor hub, 2) lift on the blade surfaces due to air foil behavior, and 3) changes in the velocity profile entering the turbine meter body. A generalized *Re*−dependent function in the form of the retarding torque term in Equation 1 is:

$$\frac{T_D}{\overline{r}^2 \rho Q^2} = C_D'(Re). \qquad (2)$$

The drag coefficient in Equation 2 is not dimensionless: geometric constants give it units of m^{-3}.

In our prior application of the ELM to turbine meter calibration data [2], we assumed that the fluid drag on the rotor surfaces was the dominant *Re*−dependent phenomenon and used the functional forms for laminar and turbulent boundary layers. The functional form for the turbulent boundary layer used was: $C_{D1}' + C_{D2}' / \log_{10} Re$. But when this function was fitted to present calibration data, the residuals at larger *Re* values were not random. We attribute this to numerous *Re*−dependent phenomena occurring in different parts of the turbine meter (blade surface, hub, tips, velocity profile), each with different length scales and transition *Re* values. Furthermore, at high rotor frequencies, the tip and hub drag terms will grow but the turbulent

boundary layer expression does not capture the growth. The complexity of these phenomena and our incomplete knowledge of the turbine's geometry make it impractical to separate these phenomena into individual terms. Therefore, in this work, to better fit the measured data in the transition and turbulent ranges we used a 3rd order polynomial in $1 / \log_{10} Re$. As in our previous work, the laminar boundary layer functional form worked well for all three turbines.

In our prior application of the ELM [2], the laminar to turbulent transition was assumed to occur at a particular *Re* value. This approach worked well for the 1.9−cm and the 1.6−cm turbines in this study too. But the 2.5−cm turbine calibration data has a broad transition region that was fitted better by including an intermittency factor $x = (Re - Re_{\text{lam}}) / (Re_{\text{turb}} - Re_{\text{lam}})$. The intermittency factor varies between 0 and 1 between Re_{lam} and Re_{turb}, and gives a linear transition over a range of *Re* values instead of at a single value [11]. Therefore the *Re*−dependent term used in this work is:

$$\frac{T_D}{\overline{r}^2 \rho Q^2} = (1-x)\frac{C'_{\text{D0}}}{Re^{0.5}} + x\sum_{i=1}^{4} C'_{Di} / (\log_{10} Re)^i$$

where $x = 0$ for $Re < Re_{\text{lam}}$,

$x = \left(Re - Re_{\text{lam}}\right) / \left(Re_{\text{turb}} - Re_{\text{lam}}\right)$ (3)

for $Re_{\text{lam}} < Re < Re_{\text{turb}}$ and

$x = 1$ for $Re > Re_{\text{turb}}$

3.2. Bearing Drag

There are three components involved in the torque due to bearing drag, T_{B} [3]: one is independent of rotor speed and has the form of Coulomb−type friction or static drag (C_{B0}), a second that increases linearly with rotor speed and is due to viscous drag in the bearing ($C_{\text{B1}} \rho \nu \omega$) and a third that increases with the square of the rotor speed, due to axial thrust and dynamic imbalance of the rotor system ($C_{\text{B2}} \omega^2$). The third component is insignificant for all the meters that we studied as expected for well−balanced rotors. The parameters C_{B0} and C_{B1} are meter specific constants that are derived in detail in our previous work [2]. They have the dimensions of kg m^2/s^2 and m^3 respectively. The bearing drag torque can be written as:

$$T_{\text{B}} = C_{\text{B0}} + C_{\text{B1}} \rho \nu \omega. \quad (4)$$

Equation 4 is rearranged in the form of the retarding torque in Equation 1, to obtain:

$$\frac{T_{\text{B}}}{\overline{r}^2 \rho Q^2} = \frac{C'_{\text{B0}}}{\rho Q^2} + \frac{C'_{\text{B1}} \nu \omega}{Q^2}, \quad (5)$$

where $C'_{\text{B0}} = C_{\text{B0}} / \overline{r}^2$ and $C'_{\text{B1}} = C_{\text{B1}} / \overline{r}^2$. Equations 3 and 5 can be inserted into Equation 1 to yield the model equation:

$$\frac{\omega}{Q} = K_{\text{i}} - C'_{\text{D}}\left(Re\right) - \frac{C'_{\text{B0}}}{\rho Q^2} - \frac{C'_{\text{B1}} \nu \omega}{Q^2}, \quad (6)$$

where the *Re*−dependent term is written as $C'_{\text{D}}(Re)$ for convenience to represent the right hand side of Equation 3. Equation 6 can be solved for *Q* to yield the working equation:

$$Q = \frac{1 + \sqrt{1 + 4\left(\frac{K_{\text{i}}}{\omega} - \frac{C'_{\text{D}}\left(Re\right)}{\omega}\right)\left(\frac{C'_{\text{B0}}}{\rho\omega} + C'_{B1}\nu\right)}}{2\left(\frac{K_{\text{i}}}{\omega} - \frac{C'_{\text{D}}\left(Re\right)}{\omega}\right)}. \quad (7)$$

For each meter, we determined the coefficients in Equation 7 from flow calibrations using liquids of various *ν*. Then, each meter can be used to measure unknown flows using the known calibration coefficients and fluid properties, and counting the frequency output by the meter.

The ELM (and Equation 7) can be written in terms of the *Ro* instead of *Re*. *Ro* has the advantage that no iteration is necessary when the flow meter is used while *Re* requires iteration because it is flow dependent. Here we use *Re* because it is the dimensionless quantity that indicates whether a flow is laminar or turbulent and it is used in the literature in empirical functions for the drag coefficient.

4. Fitting the ELM to Measured Data

Because of the complicated shape of the multiple−*ν* calibration curves, we initially fitted the model to the data by trial and error while observing the standard deviation and the minimum and maximum of the residuals. Then, we optimized the coefficients using a least squares fit algorithm. For a more detailed explanation see Ref. [2].

For each meter the coefficients that optimize the fit of the model to the measured data, the transition *Re* value for the *Re*−dependent term and the maximum *Re* value where fanning begins are listed in Table 1.

Table 1: Values for the fitted coefficients in the physical model.

	2.5 cm turbine	1.9 cm turbine	1.6 cm turbine
$Re_{K\text{peak}}$	1900	12000	3000
Re at start of fanning	3800	12000	5500
K_i [m^{-3}]	5.25×10^5	1.23×10^6	2.05×10^6
C'_{D0} [m^{-3}]	1.71×10^5	1.59×10^6	1.20×10^6
C'_{D1} [m^{-3}]	-7.19×10^5	-1.10×10^6	-1.18×10^6
C'_{D2} [m^{-3}]	8.75×10^6	1.58×10^7	1.50×10^7
C'_{D3} [m^{-3}]	-3.44×10^7	-7.32×10^7	-5.85×10^7
C'_{D4} [m^{-3}]	4.44×10^7	1.11×10^8	7.23×10^7
C'_{B0} [kg/s^2]	0.017	0.0557	0.106
C'_{B1} [m]	0.145	0.489	0.389

5. Residuals of the ELM Fits

Figures 3(a) to 3(c) show the ratio of the *K* factor calculated from our model to the measured *K* factor (the ratio of the solid lines and symbols respectively in Figure 1) for all PG+W mixtures tested for the three turbine meters in this study.

Figure 3(a) shows that for *Re* > 3500, the model fits the data from the 2.5−cm turbine within 0.11 % and for *Re* < 3500 within 1.33 %. The root mean square (RMS) deviation of the model from measured data is 0.45 %.

Figure 3(b) shows that for *Re* > 12000 ($Re_{K\text{peak}} \approx 12000$), the model fits the measured data from the 1.9−cm turbine within 0.07 % and for *Re* < 12000 within 1.67 %. The RMS deviation of the model from measured data is 0.76 %.

Figure 3(c) shows that for *Re* > 3000 ($Re_{K\text{peak}} \approx 3000$), the model fits the measured data from the 1.6−cm turbine within 0.27 % and for *Re* < 3000 within 2.29 %. The RMS deviation of the model from measured data is 0.68 %.

In the bearing−dependent region, an average curve was fit between the highest *v* curve and the lowest *v* curve. If

(a) 2.5−cm Turbine Meter

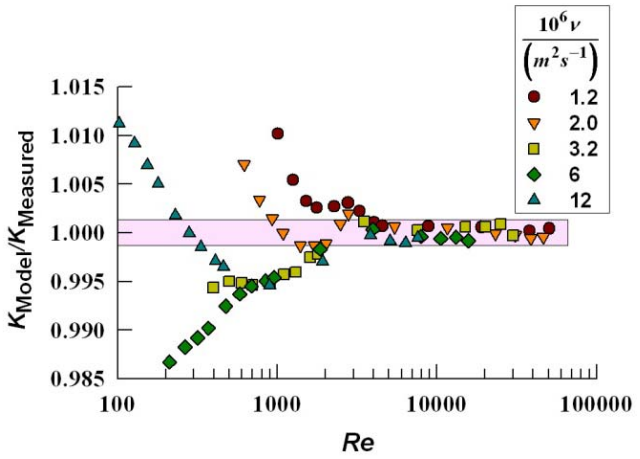

(b) 1.9−cm Turbine Meter

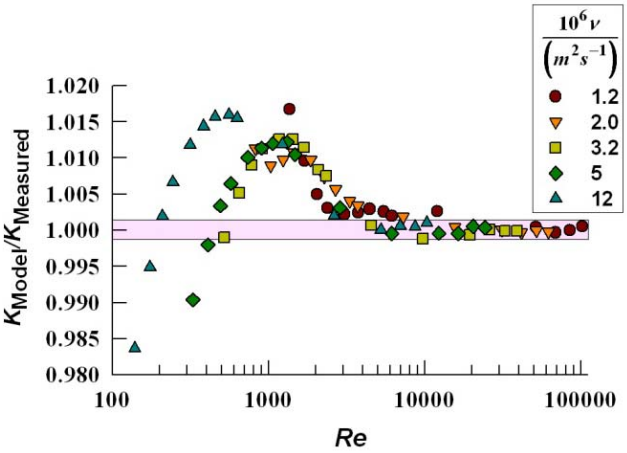

(c) 1.6−cm Turbine Meter

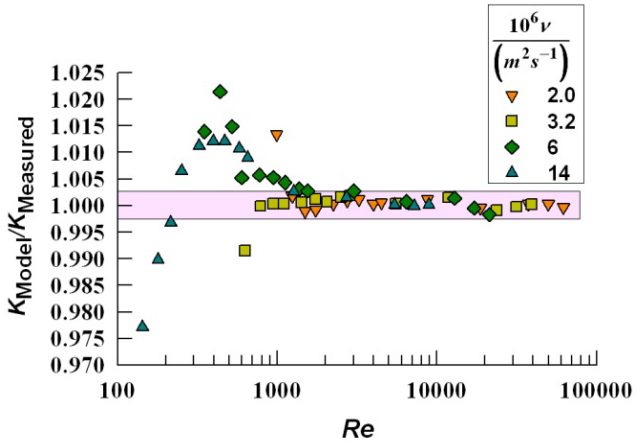

Figure 3: (a) to (c) The *K* factor calculated from the ELM divided by the measured *K* factor. (a) The ELM fits the measured data for the 2.5−cm turbine within 0.11 % at *Re* > 3500 (shaded region). (b) The ELM fits the measured data for the 1.9−cm turbine within 0.07 % at *Re* > 12000 (shaded region). (c) The ELM fits the measured data for the 1.6−cm turbine within 0.27 % at *Re* > 3000 (shaded region).

the average curve is used to predict the meter factor it will result in uncertainties as large as 3.45 % for the 2.5−cm turbine, 4.25 % for the 1.9−cm turbine and 4.76 % for the 1.6−cm turbine. Therefore, the worst fitted K factor from the model is at least two times more accurate than using an average curve approach for the multiple−ν curves. The good agreement between the fitted model and the measurements from these meters, as well as the dual−rotor meter previously modeled [2], gives us confidence that the ELM captures the major physical phenomena.

6. ELM Explains the Measured Data

The fitted ELM allows us to understand the complex behavior of the turbine meter in various flow ranges, including the fanning observed in the bearing−dependent range. The individual terms of Equation 6 are plotted in Figure 4(a) to 4(c) versus Re for each meter studied. The agreement between the fitted model and the measured data is excellent considering that the total of all model corrections are as large as 36.3 % of the ideal meter factor K_i.

Figure 4 plots the Re−dependent term, $C'_D(Re)$, the bearing static drag term, $C'_{B0}/(\rho Q^2)$, and the bearing viscous drag term, $C'_{B1}\,\omega\,\nu/Q^2$, as percentages of K_i versus Re. At $Re = Re_{K\text{peak}}$, the Re−dependent correction is at its minimum, causing the peak in the calibration curve (Figure 1) where the turbine is closest to the ideal behavior. As shown in Figure 4, the Re−dependent term dominates at the higher Re numbers and its dominance and Re−dependence leads to the ν−independent range of turbine meter performance shown in Figure 1. The Re−dependent term is consistent with the collapsing of data onto a single calibration curve on the commonly used plots of K vs. Re or Strouhal (St) vs. Ro.

The bearing static drag term is responsible for the fanning observed in the calibration curve at the lower flows shown in Figure 1. Its proportionality to $1/Q^2$ leads to several, separate curves dependent on ν when plotted vs. Re. The fanning observed in the normal presentation of turbine meter data (K vs. Re or St vs. Ro plots) is primarily a consequence of this term's dependence on flow, not Re. The fanning observed at Re values larger than $Re_{K\text{peak}}$ is clearly shown in Figure 4(a) and to a lesser extent in Figure 4(c) because the bearing static drag term still influences these turbines at $Re > Re_{K\text{peak}}$, where the transition from laminar to turbulent flow occurs (at the Re−dependent term minimum).

(a) 2.5−cm Turbine Meter

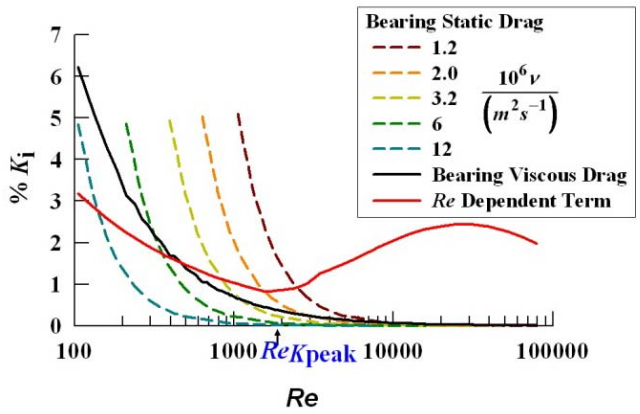

(b) 1.9−cm Turbine Meter

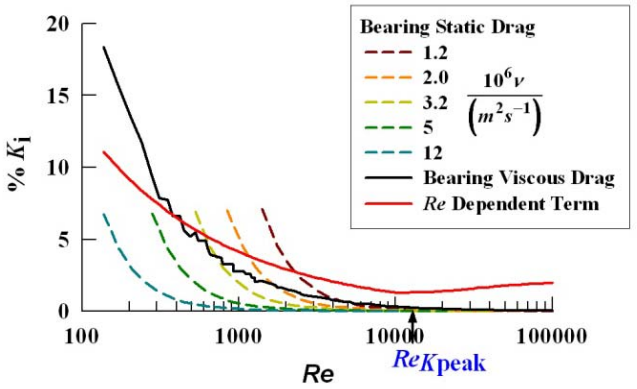

(c) 1.6−cm Turbine Meter

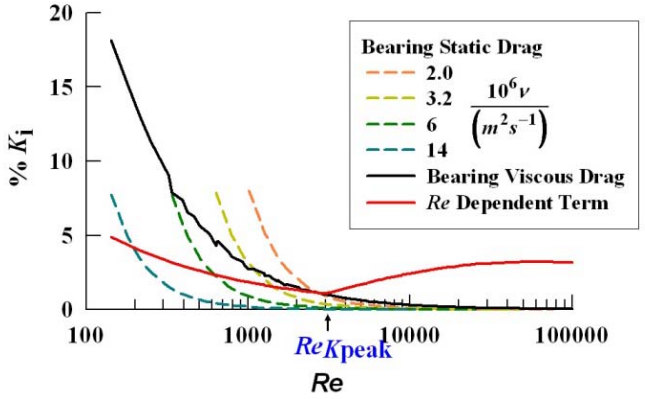

Figure 4: The individual terms of Equation 6 plotted as a percent of K_i. (a) The 2.5−cm turbine has total corrections to K_i as large as 14.2 %. (b) The 1.9−cm turbine has total corrections to K_i as large as 36.3 %. (c) The 1.6−cm turbine has total corrections to K_i as large as 30.8 %.

The bearing viscous drag correction was previously shown to have a hybrid behavior [2]: At higher Re values, it is well collapsed by Re, but the collapsing fails at lower values. An explanation for this is, at higher flows where the turbine operates near the ideal model, ω is proportional to Q and the bearing viscous drag term can be approximated by $C'_{B1}\,\nu/Q$, a term that is

proportional to 1 / *R*e and hence collapses to a single curve when plotted vs. *Re* for various *v* values. However, at low flows, the corrections to the ideal model become significant as ω is no longer proportional to *Q*, leading to a separation of the multiple−*v* curves. Hence, the bearing viscous drag term can be partially responsible for fanning of the multiple−*v* calibration curves. In contrast with our previous work, this hybrid behavior is not evident in the present measurements, probably because the present measurements do not extend to the very low values of *Re* (*Re* < 100) where the hybrid behavior was previously observed.

Each of the ELM corrections is dominant under different *Re* or *v* conditions, leading to the complex calibration curves shown in Figure 1. Because the 1.9−cm meter's calibration curves are the least complex with respect to the fanning occurring at *Re* values below the transition to laminar flow, we use it to illustrate how the correction terms explain the calibration curve's shapes. The maximum deviation between sequential *v* calibration curves was calculated and found to decrease as *v* increases. (For example: the maximum difference between the two lowest *v* curves is 7.5 % per centistoke; the maximum difference between the two highest *v* curves is 0.46 % per centistoke). The bearing static drag term dominates the other two mostly *Re*−dependent corrections at low *Re* values and at lower kinematic viscosities. Because this term is responsible for the fanning phenomenon, the fanning is strongest under these conditions. As the corrections for fluid drag and viscous bearing drag become stronger than this correction, the fanning is reduced. (For example see Figure 5).

The 2.5−cm turbine meter has the most complex calibration curves of the meters tested. The peak in the calibration curve is not coincident with the beginning of the fanning phenomenon. The peak in the calibration curves of the 2.5−cm meter occurs at *Re* ≈ 1900 but the fanning begins at *Re* ≈ 3800. This is because the transition from laminar to turbulent conditions and the flow at which bearing drag terms become significant do not coincide. This is true for the 1.6−cm meter too; the peak in the calibration curves occurs at *Re* ≈ 3000 but the fanning begins at *Re* ≈ 5500. The percent fanning was determined by the percent difference in the upper and lower calibration curves. In this region fanning at *Re* values larger than $Re_{K\text{peak}}$ is limited to less than 0.63 % for the 1.6−cm meter whereas fanning is as large as 1.60 % for the 2.5−cm meter. Fanning in the 1.9−cm meter's calibration curves only occurs at $Re < Re_{K\text{peak}}$.

Figure 6 shows the same calibration curves presented in Figure 1, however, expanded to see details near the peak and the start of the fanning of the multiple−*v* curves.

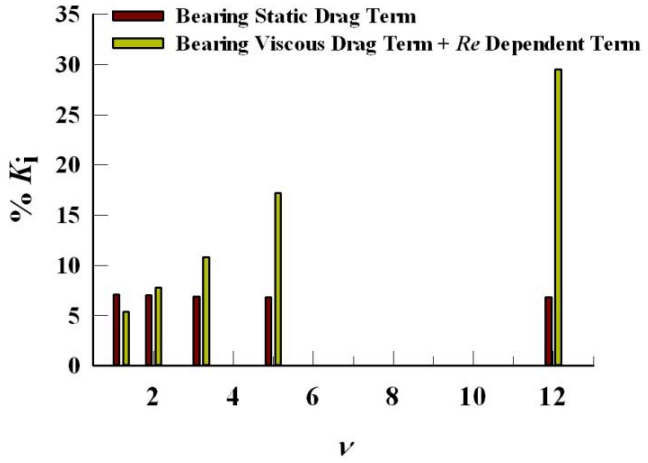

Figure 5: Contribution of correction terms for the 1.9−cm meter at the lowest *Re* tested for each *v*. The bearing static drag correction is compared to the other two corrections combined (the bearing viscous drag correction + the *Re*−dependent correction).

7. Further Investigation of Static Bearing Drag

The residuals plotted in Figure 3 are not random in the bearing−dependent range, indicating that there are observable phenomena missing from the ELM. This is not surprising given that this is the least understood part of the multiple−*v* calibration curves and until recently the reason for the fanning phenomenon was not well studied. The separation of the multiple−*v* curves produced by the fitted ELM does not exactly match the measured data in the fanning region. Because the bearing static drag term is the most significant correction in this region, we hypothesize that the physical model for the bearing static drag is incomplete. Therefore, we attempted to measure the static bearing behavior using a "bearing spin down test" under near vacuum conditions.

Examining the spin down under vacuum removes the viscous and *Re*−dependent drag forces from the rotor. If the ELM bearing static drag term is correct, the turbine frequency will decrease linearly with respect to time.

The relationship between angular acceleration and the torque associated with it is:

$$I\frac{d\omega}{dt} = T_{rotation}, \qquad (8)$$

(a) 2.5−cm Turbine Meter

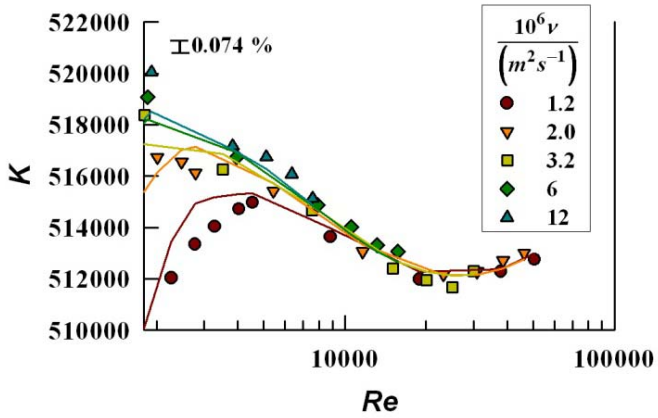

(b) 1.9−cm Turbine Meter

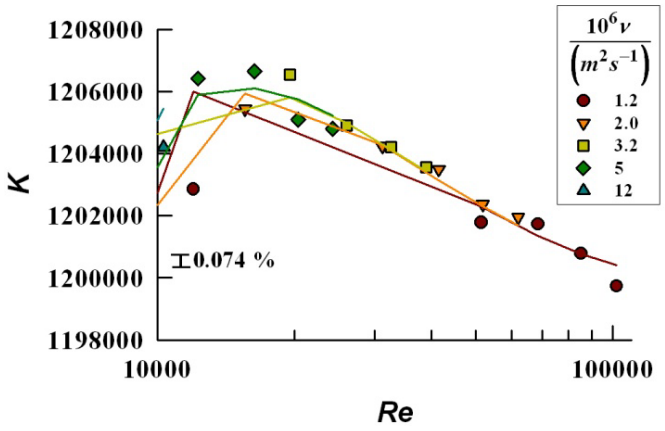

(c) 1.6−cm Turbine Meter

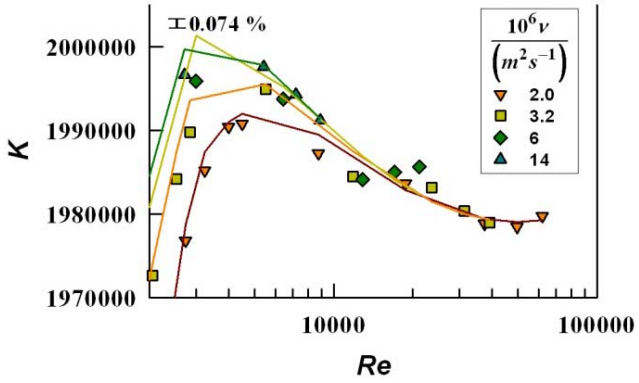

Figure 6: The calibration curves for (a) the 2.5−cm turbine, (b) the 1.9−cm turbine and (c) the 1.6−cm turbine. The error bars shown are the uncertainty of the 20−L primary standard (0.074 %). The solid lines are from the ELM and the symbols are measured data.

where I is the moment of inertia of the rotor. From the ELM, the torque imposed on the bearings is given by Equation 4. Equating the two torques gives:

$$I\frac{d\omega}{dt} = C_{B0} + C_{B1}\rho\nu\omega \qquad (9)$$

Equation 9 shows that in the absence of fluid property effects (*i.e.* vacuum), the change in angular frequency with respect to time is constant.

The experimental setup to measure the bearing spin down is shown in Figure 7(a). The spin down test was performed on the 2.5−cm meter only because the other turbines did not spin long enough to collect data. The meter was installed upstream of a vacuum pump and a large buffer volume. A valve was installed upstream of the meter. The volume was evacuated until the pressure (measured just downstream of the meter) reached a minimum (0.6 kPa to 1.0 kPa). Then the valve was opened to allow air to rapidly flow through the meter causing the rotor to spin. The vacuum was left on and the valve was closed while the turbine spun down until it stopped turning. The results of these experiments are presented in Figure 7(b). The difference between the spin down behavior in the presence of air compared to that in vacuum is due to the bearing viscous drag and the *Re*−dependent forces imposed by air on the rotor. The spin down curve under near vacuum is essentially a straight line (the curve shown has an RMS deviation from a straight line of 2.3 %, two other curves from repeated measurements have RMS deviations of 2.7 % and 0.6 %). The residuals from the fit to a straight line are random. This confirmed that in the absence of drag pertaining to fluid properties, the drag acting on the rotor is effectively constant. Therefore, the ELM imperfection in capturing fanning remains unexplained but we suspect it is because there are numerous *Re*−dependent phenomena occurring in different parts of the turbine meter (blade surface, hub, tips, velocity profile), each with different length scales and transition *Re* values.

8. Conclusions

Equation 6 is a physical model, termed the extended Lee model, or ELM, for the turbine meter that incorporates 1) fluid drag and other *Re*−dependent forces on the rotor, 2) bearing static drag, and 3) bearing viscous drag. The

model accounts for the calibration curves generated using fluids of various kinematic viscosities from a dual−rotor, 2.5−cm turbine meter [2] and single−rotor, 2.5−cm, 1.9−cm and 1.6−cm turbine meters. Using measured data from a 2.5−cm, dual−rotor meter the ELM was previously shown to correlate the volumetric flow within 0.2 % in the *v*−independent *Re* range and within 3.6 % in the bearing−dependent *Re* range despite corrections as large as 61 % of the ideal *K* factor. This gave us confidence that the model captures the major physical phenomena and can be used to understand the complex behavior of turbine meter calibration curves, particularly in the bearing−dependent *Re* range. At that time we could only speculate about how well the model might correlate measured data from meters of varying design and size. Therefore, here we tested how the ELM could be fitted to measured data from three single−rotor meters having 8 blades, 4 blades, and 6 blades with diameters of 2.5 cm, 1.9 cm, and 1.6 cm respectively.

(a)

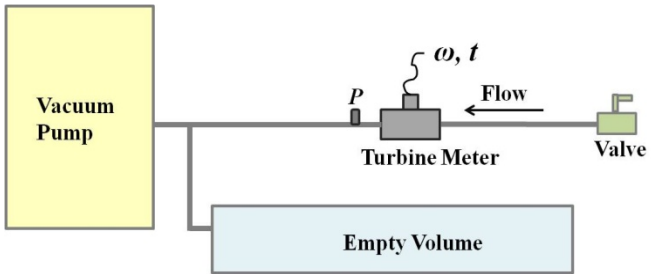

(b)

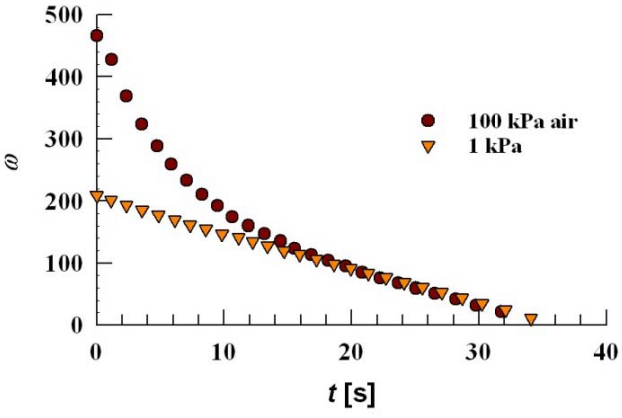

Figure 7: (a) Schematic of experimental setup to measure the spin down of the turbine meter rotor. (b) Graph of the spin down behavior of the 2.5−cm, single−rotor turbine meter in the presence of air (100 kPa) and near vacuum (≤ 1 kPa).

For metering fluids in the *v*−independent range, the ELM is not necessary for low−uncertainty flow measurements because the commonly used *St* vs. *Ro* (or *K* vs. *Re*) presentations of multiple−*v* calibration curves collapses data to within 0.1 %. This is well within the long−term reproducibility of the turbine meter. However, the ELM does greatly reduce the uncertainty in measuring low flows that are in the bearing−dependent range of the meter and it explains why changes in *v* cause fanning of the calibration curves in this range.

This paper raises the question of whether it is valuable to perform multiple−*v* calibrations on turbine flow meters in order to obtain the coefficients in the ELM. We do not recommend such a calibration because 1) as the meter ages it is likely the behavior of the bearings will change making these correction terms unstable, and 2) a multiple−*v* calibration is costly. To maintain low−uncertainty measurements that are cost effective we recommend buying a meter that operates in the *v*−independent range for the application at hand. However, calibrations at a minimum of two kinematic viscosities are valuable, not for determining ELM coefficients, but for identifying where fanning begins so that the meter is only used in the *v*−independent range.

Acknowledgements

This work was partially sponsored by the U.S. Department of Defense Physical / Mechanical Calibration Coordination Group.

References

[1] Measurement of Liquid Hydrocarbon by Turbine Meter Systems. American Petroleum Industry Standard 2534, 1970.

[2] Pope JG, Wright JD, Johnson AN, Moldover MR. Extended Lee Model for the Turbine Meter and Calibrations with Surrogate Fluids. Flow Measurement and Instrumentation, 2012; 24: 71 – 82.

[3] Lee WFZ, Evans, HJ. Density Effect and Reynolds Number Effect on Gas Turbine Flowmeters. Journal of Basic Engineering, 1965; 1043 − 57.

[4] Lee WFZ, Karlby H. A Study of Viscosity Effect and Its Compensation on Turbine-Type Flowmeters. Journal of Basic Engineering, 1960; 717 − 27.

[5] Rubin M, Miller RW, Fox WG. Driving Torques in a Theoretical Model of a Turbine Meter. Journal of Basic Engineering, 1965; 413 − 20.

[6] Baker RC. Turbine flowmeters: II. Theoretical and Experimental Published Information. Flow Measurement and Instrumentation, 1993; 4: 123 − 44.

[7] Johnson AN, Crowley CJ, Yeh TT. Uncertainty Analysis of NIST's 20 Liter Hydrocarbon Liquid Flow

Standard. Journal of the Metrology Society of India, 2011; 26: 187 − 202.
[8] Yang C, Ma P, Tang D, Jin F. Excess Molar Volume, Viscosity and Heat Capacity for the Mixture of 1,2 − Propanediol − Water at Different Temperatures. Chinese J. Chem. Eng., 2003; 11: 175 − 80.
[9] Jimenez J, Martinez F. Study of Some Volumetric Properties of 1,2-Propanediol + Water Mixtures at Several Temperatures. Rev. Col. Cienc. Quim. Farm., 2005; 1: 46 − 57.
[10] Wadlow D. Turbine and Vane Flowmeters, In: J.G. Webster, editors. The Measurement, Instrumentation and Sensors Handbook, Boca Raton, FL: CRC Press; Dec. 1998; Chapter 28.4.
[11] Tennekes H, Lumley JL. A First Course in Turbulence. MIT Press, 1972.